Published in final edited form as:

ACS Appl Mater Interfaces. 2016 March 23; 8(11): 7403–7410. doi:10.1021/acsami.6b01188.

In-situ Grown TiO_2 Nanospindles Facilitate the Formation of Holey Reduced Graphene Oxide by Photodegradation

Guiming Peng[†,‡,§,±], **James E. Ellis**[‡], **Gang Xu**[*,§], **Xueqing Xu**[§], and **Alexander Star**[*,‡]

[†]School of Metallurgy and Chemical Engineering, Jiangxi University of Science and Technology, Ganzhou, 341000, Jiangxi, China.

[‡]Department of Chemistry, University of Pittsburgh, Pittsburgh, Pennsylvania, 15260, USA.

[§]CAS Key Laboratory of Renewable Energy, Guangzhou Institute of Energy Conversion, Chinese Academy of Sciences, Guangzhou, 510640, China.

[±]University of Chinese Academy of Sciences, Beijing, 100049, China.

Abstract

Titanium dioxide (TiO_2) nanostructures and TiO_2/graphene nanocomposites are intensively studied materials for energy conversion, energy storage, and organic contaminant photodegradation. However, for TiO_2/graphene composites, impermeability across the graphitic basal plane for electrolytes, metal ions, and gas molecules hinders their practical applications. Herein we report a simple, environmentally-friendly synthetic route for mesoporous anatase TiO_2 nanospindles, and successfully apply this method to obtain in-situ grown TiO_2 nanospindles/graphene oxide composite. After a thermal reduction at 400 °C, holes are created in the reduced graphene oxide (RGO) sheets through a photocatalytic oxidation mechanism. The formation of holes in RGO is promoted by photogenerated hydroxyl radicals that oxidize and subsequently decarboxylate the graphitic surface of RGO. The proposed mechanism was supported by photocatalytic electrochemical properties of the nanomaterials. The resulting TiO_2/holey RGO composites may overcome the original impermeability of graphene sheets and find applications in catalysis, energy conversion/storage devices, and sensors.

Keywords

graphene; carbon nanotubes; titanium dioxide; oxidation; catalysis; oxygen reduction reaction

[*]**Corresponding Author** Address correspondence to astar@pitt.edu.

ASSOCIATED CONTENT

Supporting Information: TEM images of TiO_2 nanospindles, TiO_2/carbon nanotubes and TiO_2/graphene oxide composites; methyl orange (MO) photodegradation using the TiO_2 nanospindles and commercial P25 catalyst; changes in Raman D/G ratios of TiO_2/RGO during photodegradation; ratios of various carbon functionalities deconvoluted from the C1s XPS spectra of TiO_2/RGO; chronoamperometric response of TiO_2/RGO; commercial Pt/C to UV illumination and Koutechy-Levich (K-L) equation and calculated transferred electron number in oxygen reduction reaction (ORR). This material is available free of charge via the Internet at http://pubs.acs.org.

INTRODUCTION:

Titanium dioxide (TiO_2) has been attracting considerable interest because of its excellent physical and chemical stability, low cost, nontoxicity and wide applications in hazardous substance photodegradation,[1, 2] solar energy conversion,[3–6] and sensing.[7] However, inferior conductivity within TiO_2 networks hampers their practical applications.[8] To this end, compositing TiO_2 with conductive nanomaterials, such as carbon nanomaterials, is significant to enhance the practical properties of TiO_2.

Among various TiO_2-based composites, TiO_2 modified graphene is intensively studied for advanced electrocatalysts, solar energy conversion materials, and lithium ion batteries.[9–12] Graphene, a one-atom-thick nanomaterial, possesses remarkable electrical conductivity, large surface area, and outstanding chemical stability.[13, 14] Therefore, graphene in TiO_2/graphene composites is able to overcome the low conductivity of TiO_2, and allow photogenerated electrons to be conducted more efficiently. Compared with physically blending both compounds together, in which weak interaction between TiO_2 and graphene is a main drawback, in-situ anchoring TiO_2 nanoparticles onto graphene via chemical bonds improves the stability of the composite and promotes charge separation and mutual electron transport between TiO_2 and graphene.[9, 15] Furthermore, TiO_2 nanoparticles on the support prevents graphene sheets restacking,[10] which is beneficial for increasing the composite specific surface area and affording more access for electrolyte and gas molecules. The ability to control size, morphology, and dispersion density of inorganic nanocrystals on graphene sheets, allowing one to tailor the material toward a specific application,[10, 14, 16, 17] is still an important challenge, and calls for more efforts.

For graphene-based materials, rapid diffusion of electrolyte and gas molecules through graphene and its composites is another issue that needs to be addressed. Hierarchically porous structured graphene composites are reported to be effective supercapacitors and photocatalysts by constructing extra tortuosity and wrinkles.[9, 18, 19] However, the impermeability across the graphene basal plane for electrolytes and gas molecules remains a challenge. A graphene structure with holes throughout (i.e., holey graphene) affords interlayer transport pathways across the graphene plane and ultimately to the inner electrode surfaces for electrolyte and Li-ions, thus overcoming the inherent impermeability of graphene.[20] However, the reported methods to prepare holey graphene are either not scalable, require toxic or hazardous reagents, or involve harsh reaction conditions.[12, 20–22] A more scalable and accessible synthetic route for holey graphene needs to be developed.

Furthermore, since TiO_2/graphene is widely used as a photocatalyst,[11, 15, 18, 23] in addition to the catalysis performance, the photochemical stability of the composite is another issue that should be taken into account. TiO_2/graphene oxide composite was confirmed to be chemically unstable and could be reduced in ethanol upon UV-light irradiation.[8, 24, 25] Since TiO_2/reduced graphene oxide composites in water can be mineralized by UV-light in oxygen-abundant conditions,[26] an important question concerning graphene-based composites can be raised: Is graphene a stable support for photocatalysis? Recently, Kamat *et al.* have investigated mechanically mixed TiO_2/RGO composites for this mineralization process,[26] but the effect of covalently linked TiO_2/RGO composites with different shaped

nanocrystals are still unexplored. Thus it can be seen, further investigation and mechanistic insights into TiO_2/graphene composites, including material synthesis and photochemical stability toward UV-light are necessary.

To date, most of the reported methods to obtain TiO_2 modified graphene are time- and energy-consuming hydrothermal methods.[9, 27] Here, we report a simple, surfactant-free, low temperature process to synthesize mesoporous TiO_2 nanospindles. Following the same procedure, the TiO_2 nanospindles were chemically anchored onto graphene oxide (GO) to form a TiO_2/GO composite. The TiO_2 nanospindle dispersion density on GO sheets is tunable by changing the titanium precursor amount. After a thermal reduction to form TiO_2/reduced GO (TiO_2/RGO), the TiO_2/RGO was further transformed into holey RGO via a simple UV light irradiation when bubbling O_2. Longer time exposure of the TiO_2/RGO to UV light, finally, caused degradation of the RGO into photo-oxidized RGO nanosheets. The photo-oxidation mechanism was investigated by X-ray photoelectron spectroscopy (XPS), Raman spectroscopy, and electrochemistry. The photo-instability of TiO_2/RGO affords a unique way to produce holey RGO, which is beneficial for this material's use in energy conversion and storage field by overcoming the impermeability across the graphene basal plane for electrolyte and Li-ions.

EXPERIMENTAL SECTION

TiO_2 nanospindles synthesis:

TiO_2 nanospindles were synthesized by adding 10 μL titanium isopropoxide (TTIP) into 3 mL HCl aqueous solution (0.5 mol/L), which was then diluted by 1 mL deionized water. After 5 minutes sonication, the solution was incubated at 90 °C for 1 hour. Afterward, the precipitate was collected by centrifugation and washed with deionized water until the pH reached 7. Finally, the TiO_2 nanospindles suspension was freeze-dried. To increase the TiO_2 crystallinity, the powder was annealed at 400 °C in N_2 atmosphere for 30 minutes.

TiO_2 nanospindles/reduced graphene oxide synthesis:

TiO_2 nanospindles/GO were synthesized by adding 1 mL GO aqueous solution (0.02 mg/mL) into 3 mL HCl aqueous solution (0.5 mol/L) followed by 5 minutes sonication. Then, 10 μL titanium isopropoxide (TTIP) was injected into the above mixture. The reaction condition and product collection process were the same as the previously mentioned TiO_2 nanospindle synthesis. Then the obtained composite underwent a dual functional anneal at 400 °C in N_2 atmosphere for 30 minutes to form TiO_2/RGO. The synthesized materials and their chemical and structural transformations during photo-oxidation were characterized using transmission electron microscopy (TEM), X-ray diffraction (XRD) spectroscopy, Raman spectroscopy, XPS, atomic force microscopy (AFM), and electrochemistry.

Material Characterization:

Low-resolution TEM images were obtained with a Philips/FEI Morgagni at an accelerating voltage of 80 kV. High-resolution TEM images were taken using JEOL 2100F microscope with an accelerating voltage of 200 kV. TEM samples were prepared by drop-casting an aqueous solution of the nanomaterial on a lacey carbon TEM grid (Pacific Grid-Tech) for

low-resolution TEM imaging or on C-FLAT holey TEM grid (Electron Microscopy Sciences) for high-resolution TEM imaging. AFM images were collected using a Veeco Dimension 3100 (Plainview, NY) multimode scanning probe microscope in tapping mode for height, phase, and sectional analysis. AFM samples were prepared on freshly cleaved mica sheets. Approximately 10 μL of sample was spin-coated at 1400 rpm and allowed to dry in ambient prior to imaging.

XPS spectra were collected on Thermo Scientific K-Alpha X-ray photoelectron spectrometer using monochromated Kα X-rays (1486.6 eV). XPS samples were prepared by briefly sonicating the nanostructures in ethanol and dropcasting them onto an aluminum substrate, and allowing the solvent to evaporate completely. The sample spot size was 400 μm, with a pass energy of 200 eV for the survey scans and 50 eV for high resolution. Charge compensation was provided by a low-energy electron source and Ar^+ ions. The spectra were fitted after background subtraction of a Shirley type baseline. Peak shapes were fitted using a Gaussian:Lorentzian ratio of 80:20. The FWHM was set within the range 1.5 – 3.0. Raman spectra were collected on a Reinshaw inVia Raman microscope at an excitation wavelength of 633 nm with scan wavelength range from 1000 to 2000 cm^{-1} at 10% laser power (maximum 17 mW) with 15 s exposure time. Samples were dropcasted on a quartz slide and dried before characterization.

All electrochemical measurements including cyclic voltammetry (CV), rotating ring disc electrochemistry (RRDE), linear sweep voltammetry (LSV), and chronoamperometry measurements were performed using a CHI 7042 Bipotentiostat (CH Instruments, Austin, TX). A Pt wire electrode (CHI 115) and an Ag/AgCl (CHI 111, 1 M KCl) electrode were used as the counter and reference electrode, respectively. All potentials are reported with respect to Ag/AgCl. The electrodes were purchased from CH Instruments, Austin, TX. The RRDE was purchased from Pine Instrument Company (AFE7R9GCPT; reported collection efficiency, N = 0.37) containing a glassy carbon (GC) disk and Pt ring electrode. The RRDE experiments were performed on a MSR Electrode Rotator.

RESULTS AND DISCUSSION

Free TiO_2 nanospindle characterization:

TEM images of the synthesized free TiO_2 nanospindles are presented in Figure 1 and Figure S1. Before calcination, the TiO_2 nanopartiles exhibit unique nanospindle morphology with the length of ~45 nm and width of ~15 nm (Figure 1a). The XRD spectrum indicates that most of these nanospindles are anatase phase with a coexisting part rutile phase (blue curve in Figure 1d). After annealing at 400 °C for 30 minutes, the shape of these nanospindles remained largely unchanged although slight deformation took place during the calcination process (Figure 1b). Interestingly, two to three ~7 nm-sized voids could be observed in each TiO_2 nanospindle (Figure 1b) after calcination. The voids likely originated from the volume contraction and H_2O removal during annealing. In addition, the selected area electron diffraction (SAED) pattern (inset in Figure 1c) and the lattice interspacing of 3.4 Å and 2.5 Å could be assigned to the (101) and (004) of anatase phase, respectively (Figure 1c).[9, 28] The XRD spectra of the calcinated TiO_2 nanospindles matched the standard anatase pattern (JCPDS 002–0387). Both the high resolution TEM (HRTEM) and the increased XRD peak

intensity (Figure 1d) indicated the improved crystallinity of the TiO_2 nanospindles by calcination. Methyl orange (MO) photodegradation performance was evaluated on the free mesoporous TiO_2 nanospindles by monitoring the MO concentration while illuminating the MO solution with 254 nm UV light under stirring. Relative to smaller-sized P25, comparable degradation rate was obtained with the TiO_2 nanospindles (Figure S2).

Control experiments were performed to track the TiO_2 nanospindle growth process. TiO_2 nanospindle morphology, including the size and shape, remained the same even though the growth duration was elongated to 3 hours while keeping other conditions constant (Figure S1a). When the TTIP amount was doubled to 20 μL, well dispersed relatively bigger TiO_2 nanospindles with length of ~50 nm, and width of ~20 nm were obtained (Figure S1b). However, the alteration of the acidity of the reaction mixture greatly changes the nanoparticle shape (Figure S1c and S1d). Agglomerated unshaped nanoparticles formed in the neutral solution (Figure S1c), while dispersed unshaped nanoparticles were synthesized in 0.75 mol/L HCl solution (Figure S1d). Judging from the above results, HCl plays two roles in the reaction: (i) to suppress and slow down the hydrolysis rate of TTIP and (ii) to induce the formation of uniquely-shaped nanospindles.

As discussed above, the synthesis method for anatase TiO_2 nanospindles described in this publication involves no toxic reagents. Compared with the previously reported hydrothermal methods where the reaction temperature was above 150 °C and took more than 30 hours,[27] the synthesis process here is conducted below 100 °C and requires only 1 hour for the synthesis process. Besides these merits, the facile process to synthesize anatase mesoporous TiO_2 nanospindles could also be adopted to grow such TiO_2 nanospindles onto various supports, such as graphene oxide (Figure 2) and oxidized carbon nanotubes (Figure S3).

TiO_2 nanospindles/reduced graphene oxide characterization:

We employed the same synthesis process as the TiO_2 nanospindles except replacing the deionized water with 0.02 mg/mL GO solution to grow TiO_2 nanoparticles onto the graphene oxide sheets. Surprisingly, although the size increased slightly in terms of length (~100 nm) and width (~30 nm), the nanospindle-shaped morphology of the TiO_2 nanoparticles remained unchanged, while the nanospindles were distributed evenly onto the graphene oxide sheets (Figure S4). After annealing and thermal reduction, the mesoporous structure and anatase phase for the TiO_2 nanospindles on RGO (inset in Figure 2a) are similar to the free nanospindles in Figure 1b. It is noted that free unattached nanospindles could not be observed under these conditions. This phenomenon indicated that, compared with homogeneous growth in the solution, the nanospindles prefer to nucleate at the defect sites (oxygen-containing moieties) on the GO sheets. In addition, the population of the nanospindles could be tuned by varying the TTIP amount (Figure S5), which is significant for tailoring the behavior of such composite to its application.

Moreover, it is reported that GO shows deteriorated electrical conductivity because of the disrupted sp^2 carbon network.[21, 29] Electrical conductivity of GO can be recovered by restoring sp^2 conjugation via GO reduction. Thermal reduction to deoxygenate the oxygen-containing moieties from GO is reported to take place at around 180 °C,[29, 30] while graphene basal planes can endure 480 °C before reacting with O_2 in hot air.[20] Therefore, the

TiO_2/GO is actually deoxygenated without basal plane decomposition while calcinating at 400 °C in N_2 atmosphere in this study (denoted as TiO_2/RGO). The high temperature endurance of TiO_2/RGO is also confirmed by TEM in Figure 2a, where the integrity of the support material sheets remains without any pores post-calcination.

Raman spectra were recorded and presented in Figure 3a. In accordance with XRD and HRTEM (Figure 1c, 1d, and 2a), both the free TiO_2 nanospindles and TiO_2/RGO exhibited anatase Raman characteristics. For the free TiO_2 nanospindles, the main E_g vibration peak is centered at 144 cm^{-1}, while the vibration peaks at 399 cm^{-1}, 516 cm^{-1}, and 640 cm^{-1} are assigned to B_{1g}, A_{1g}, and E_g modes of anatase phase, respectively.[15, 31] Comparing with those Raman peaks of free TiO_2 nanospindles, the main E_g vibration peak of TiO_2/RGO is blue-shifted to 156 cm^{-1}, while the peak at 394 cm^{-1} is red-shifted. The Raman peak shifts indicate the strong interaction between the TiO_2 nanospindles and the RGO, which promote the charge separation and electron transport.[1, 15]

X-ray photoelectron spectroscopy (XPS) was used to track the change of oxygen containing groups in GO in TiO_2/GO. As is shown in the high resolution XPS of C1s (Figure 3b), before calcination, two typical peaks of GO located at 284.18 eV and 286.27 eV are usually assigned to C-C and C=C, and C-O bond, respectively.[32] By deconvolution, C=O bond at 287.92 eV, C(=O)-O bond at 290.10 eV, and defect-containing sp^2 carbon at 285.15 eV are discerned, which prove that various oxygen-containing groups exist in the GO.[32] The presence of the oxygen-containing groups afford nucleation sites and directly react with TTIP to form TiO_2 nanospindles, which is also certified by the TiO_2 Raman peak shift due to strong interaction with GO. Comparing the C1s XPS spectra for the samples before and after calcination, the amount of oxygen-containing groups disappeared while the defect containing sp^2 carbon bond amount increased after calcination (Figure 3b, Table S1). Therefore, when annealing the TiO_2/GO at 400 °C in N_2 to increase the crystallinity of TiO_2, thermal reduction of GO takes place simultaneously.

Photochemical stability study of RGO in TiO_2/RGO:

Since the TiO_2/RGO composites are frequently used in photocatalysis or photovoltaics, the photochemical stability of such catalyst is of much significance. For the photochemical stability experiment, O_2 was bubbled into the TiO_2/RGO suspension (0.05 mg/ml in water) under stirring while illuminating with 254 nm UV light for a series of timed durations. Interestingly, after 8 hours UV illumination, the RGO was photodegraded to some extent, and many holes appeared in the RGO sheets as indicated by the arrows in Figure 2b. In addition, compared with the initial material in Figure 2a, the TiO_2 nanospindles were more sparsely distributed on the RGO sheet (Figure 2b). TiO_2/RGO, after 8 hour photodegradation, was characterized by AFM with the image presented in Figure 2d. Holes were observed over the whole RGO sheet, where the TiO_2 nanospindles also could be discerned. At this stage, the size of most holes ranged from 50 nm to 150 nm (Figure 2d, S6). The thickness of the RGO sheets was ~1.5 nm (inset in Figure 2d), corresponding to a single layer.[21] This height is larger than the theoretical value of ~0.8 nm because of the oxygen containing functionalities on both sides.[33] When further exposing the composite to

UV light for 18 hours, the RGO sheets were decomposed into separate smaller pieces (smaller than 200 nm) with fewer TiO_2 nanospindles attached on the edges (Figure 2c).

Therefore, like photodegradation of MO on TiO_2 nanospindles, these results reveal that the presence of TiO_2 causes decomposition of RGO in TiO_2/RGO. Photodegradation for 8 hours evolved TiO_2 nanospindles/RGO into holey RGO with TiO_2 nanoparticles on it. Judging from the photodegradation kinetic behavior, pore size can be tuned by varying the UV irradiation time before the RGO decomposes into separate sheets. Due to the extra access across the graphene basal plane for electrolyte, metal ions, and gas molecules, such TiO_2/holey RGO composites would be beneficial for energy storage and conversion applications such as lithium batteries, ultracapacitors, and photocatalysts.[20, 34]

Raman spectroscopy of TiO_2/RGO was performed at different UV irradiation durations and plotted in Figure 3a. Relative to the G band intensity, the anatase Raman peak intensity decreased gradually as the time progressed. This is probably because the TiO_2 nanospindles detached from the RGO due to the prior degradation at the interconnection sites (Figure 2a-c). Since the TiO_2 nanospindles preferred to grow starting from the defective sites,[9, 15] both the nanospindle detachment observed from TEM images and decreased TiO_2 Raman intensity proved that the defective sites were more prone to reaction with the generated free radicals and reactive oxygen species (ROS). Apart from the above-discussed anatase characteristic peaks, the peak at 1333 cm^{-1} is associated with the disordered sp^2 carbon and is commonly named D band, while the peak at 1596 cm^{-1}, G band, is related to the well-ordered graphite.[22, 32] The D/G intensity ratio reflects the extent of structural disorder of the graphitic material.[35] According to the obtained Raman spectra (Figure 3a), the D/G ratio was calculated and plotted as a function of UV irradiation time in Figure S7. The D/G ratio increased almost linearly from initial value of 1.06 to 1.18 after 18 hours photodegradation (Figure S7). The increase in D/G ratio disclosed that the photodegradation introduced more defects into the graphitic substrate. To verify the introduced defects during the photodegradation, the C1s XPS spectra of the sample after 18 hours UV irradiation were recorded in Figure 3b. It was found that C-O, C=O, and C(=O)-O bonds were recovered along with slightly increased defect-containing sp^2 carbon during the photodegradation (Figure 3b, Table S1), which was consistent with the increase of D/G ratio.

To gain insight into RGO photodegradation in TiO_2/RGO, photo-catalytic electrochemical behavior on the surface of TiO_2 nanospindles is a critical factor that should be taken into account. To this end, a catalyst ink composed of 1 mg/mL TiO_2 nanospindles and 10 μL 25% Nafion was prepared for electrochemical characterization in oxygen reduction reaction (ORR). 10 μL of such catalyst ink was drop-casted onto a glassy carbon electrode. The corresponding cyclic voltammogram (CV) curves in O_2 saturated 0.1 mol/L KOH are depicted in Figure 4a. As can be seen from the CV curves, the TiO_2 nanospindles show a prominent O_2 reduction peak at the potential of –0.42 V (vs Ag/AgCl). In order to monitor the same condition as the TiO_2/holey RGO evolution, 254 nm UV light was used to illuminate the catalyst when testing the electrochemical performance. Interestingly, the reduction current increased almost one third under the UV light illuminated condition. The enhanced oxygen reduction current can also be detected by the chronoamperometry when keeping the electrode potential at –0.42 V (Figure S8). Specifically, the reduction current

increased rapidly from 1.25×10^{-5} A to 2.46×10^{-5} A upon the UV light being turned on, followed by a slow decay to the stable current of 1.98×10^{-5} A. Once the UV light was off, the reduction current dropped to the initial value. Therefore, oxygen reduction reaction (ORR) on TiO_2 nanospindles is promoted by UV light at the applied potential of –0.42 V. This is probably because: (i) photogenerated electrons by TiO_2 could be used to reduce O_2 or (ii) a small amount of O_2 could be yielded by the water splitting on TiO_2 which increases the O_2 concentration in the solution and promotes ORR.

To detect the electron transfer number in the oxygen reduction process on the TiO_2 nanospindles, linear sweep voltammograms (LSV) were conducted at various rotating rates (from 300 to 2500 rpm) (Figure 4b). Similar to the CV curves in Figure 4a, the nonzero cathodic currents started at ~–0.3 V and reached the limiting peak current in the range between –0.4 V and –0.45 V. The peak reduction current increased as the rotation rate increased, which is mainly due to the increased diffusion efficiency. Then the electron transfer number was calculated according to the Koutechy-Levich (K-L) equation, which is detailed in the Supporting Information. The corresponding K-L plots were demonstrated in Figure 4c, while the calculated electron transfer numbers at different potentials were shown in Figure S9. Clearly, electron transfer number at – 0.42 V is only 2.35, which means that the oxygen reduction process on the as-prepared TiO_2 nanospindles is more like a 2-electron process, and most of the reduction intermediate product is H_2O_2.

The electrocatalytic ORR activity of TiO_2 in TiO_2/RGO is closely related to surface catalytic reactions involving molecular oxygen and the reactive intermediates such as OH, OOH, and O for the complete $4e^-$ reaction, and OOH and HOOH for the incomplete two-step $2e^-$ reaction.[36] The measured electron transfer number of 2.35 supports the fact that the incomplete two-step $2e^-$ reaction occurs, where hydrogen peroxide is formed and desorbed from the catalysts surface. Coincidently, the in-situ generated hydrogen peroxide can undergo homolytic cleavage to form highly reactive hydroxyl (•OH) radical and the introduction of ultraviolet (UV) irradiation to the system accelerates the formation of this radical species.[37, 38] On the other hand, as evidenced by the increased ORR activity of TiO_2 nanospindles with UV light irradiation (Figure 4a), photogenerated electrons on the surface of TiO_2 can react with oxygen in aqueous solution. Based on the calculated electron transfer number, O_2 adsorbs on the surface of the photo-excited TiO_2 nanospindles as the intermediate OOH. The sequestering of photogenerated electrons in the form of OOH will slow down the electron-hole recombination rate, allowing a longer lifetime for photogenerated holes to react with water. Strong oxidant hydroxyl radicals form via combination of photogenerated holes and OH^-, as shown in Figure 5. The resultant hydroxyl radicals would preferentially attack the defective sites in the graphitic material,[26] which also happen to be the connecting points between the TiO_2 nanospindles and the RGO sheets. Thus, TiO_2 nanospindles are observed to produce holes in and detach from RGO during the photodegradation procedure. Reactive hydroxyl radicals can oxidize graphitic carbon nanomaterials (i.e., carbon nanotubes and graphene) by previously reported chemical transformations of their oxygen functional groups.[39] First, hydroxyl radicals impart carboxylic acids at the defect sites, and these oxygen moieties are subsequently further oxidized to CO_2 and H_2O. Next, hydroxyl defect sites are converted into quinones. Finally, the strong oxidizing local environment facilitates the conversion of the quinone groups to

carboxylic acids, which can undergo further decarboxylation. The net result of these oxidation reactions is a breakage of the underlying C−C bonds and overall degradation of graphitic carbon nanomaterial. In this work, RGO already consists of sp^3-hybridized defects with oxygen functional groups, including tertiary alcohols on the basal plane and carboxylic acid and keto groups on the edge (Figure 5).[40] We hypothesize that in a similar fashion as was previously reported for graphene oxide degradation by photo-Fenton reaction,[41] hydroxyl radicals formed in the vicinity of the TiO_2 nanospindles will oxidize RGO via (i) the conversion of oxygen moieties to higher oxidation states, resulting in decarboxylation, and (ii) electrophilic addition to unsaturated bonds (i.e., nonoxidized sp^2 segments that are either aromatic or conjugated), which creates more oxygen defect sites.

CONCLUSION:

In conclusion, mesoporous TiO_2 nanospindles were synthesized via a surfactant-free, low temperature, environmentally-friendly method. 0.5 M HCl aqueous solution was confirmed as a critical factor, which slowed down the hydrolysis rate of TTIP and controlled the TiO_2 morphology to be nanospindle. The identical synthesis process was successfully transferred to anchor the TiO_2 nanospindles onto the graphene oxide (TiO_2/GO). Using the TiO_2/GO composite, TiO_2/holey RGO was obtained via a thermal reduction followed by a photocatalytic oxidation reaction. A two-electron electrocatalysis of oxygen reduction reaction measured for these nanostructures supported the proposed mechanism for the hole formation in graphene under UV illumination. This facile and scalable methodology to prepare TiO_2/holey RGO composite has potential in improving the nanocomposite volumetric capacitive performance for energy conversion and storage applications. The photo-instability of TiO_2/RGO also indicates extra consideration is needed when applying this material in solar cells and photocatalysis.

Supplementary Material

Refer to Web version on PubMed Central for supplementary material.

ACKNOWLEDGMENT

This work was partially supported by NIEHS Award R01ES019304 and NSF CAREER Award No. 0954345. G.P. is thankful for the support from the State Scholarship Fund of China Scholarship Council, Scientific Research Fund for Advanced Talents of Jiangxi University of Science and Technology (jxxjbs15023), and the Project on the Collaborative Innovation and Environmental Construction Platform of Guangdong Province (2014A050503051). The authors thank the Nanoscale Fabrication and Characterization Facility (NFCF) and the department of biology from the University of Pittsburgh for provision of access to instruments and Dr. Susheng Tan (NFCF) and Gregory J. Morgan for their assistance with HRTEM.

REFERENCES

(1). Zhang L-W; Fu H-B; Zhu Y-F Efficient TiO2 Photocatalysts from Surface Hybridization of TiO2 Particles with Graphite-Like Carbon. Adv. Funct. Mater 2008, 18, 2180–2189.

(2). Liu M; Piao L; Zhao L; Ju S; Yan Z; He T; Zhou C; Wang W Anatase TiO_2 Single Crystals with Exposed {001} and {110} Facets: Facile Synthesis and Enhanced Photocatalysis. Chem. Commun 2010, 46, 1664–1666.

(3). Peng G; Xu X; Mei F; Xu G; Wu J; Gao D; Ellis JE; Zhao Y; Xing Y; Star A Substrate Placement Angle-Dependent Growth of Dandelion-Like TiO2 Nanorods for Solid-State Semiconductor-Sensitized Solar Cells. RSC Adv 2014, 4, 53335–53343.

(4). Peng G; Wu J; Zhao Y; Xu X; Xu G; Star A Ultra-Small TiO2 Nanowire Forests on Transparent Conducting Oxide for Solid-State Semiconductor-Sensitized Solar Cells. RSC Adv 2014, 4, 46987–46991.

(5). Cho IS; Chen Z; Forman AJ; Kim DR; Rao PM; Jaramillo TF; Zheng X Branched TiO_2 Nanorods for Photoelectrochemical Hydrogen Production. Nano Lett 2011, 11, 4978–4984. [PubMed: 21999403]

(6). Peng G; Wu J; Wu S; Xu X; Ellis JE; Xu G; Star A; Gao D Perovskite Solar Cells Based on Bottom-Fused TiO_2 Nanocones. J. Mater. Chem. A 2016, 4, 1520–1530.

(7). Ding M; Sorescu DC; Star A Photoinduced Charge Transfer and Acetone Sensitivity of Single-Walled Carbon Nanotube-Titanium Dioxide Hybrids. J. Am. Chem. Soc 2013, 135, 9015–9022. [PubMed: 23734594]

(8). Qiu J; Zhang P; Ling M; Li S; Liu P; Zhao H; Zhang S Photocatalytic Synthesis of TiO2 and Reduced Graphene Oxide Nanocomposite for Lithium Ion Battery. ACS Appl. Mater. Interfaces 2012, 4, 3636–3642. [PubMed: 22738305]

(9). Qiu B; Xing M; Zhang J Mesoporous TiO_2 Nanocrystals Grown in Situ on Graphene Aerogels for High Photocatalysis and Lithium-Ion Batteries. J. Am. Chem. Soc 2014, 136, 5852–5855. [PubMed: 24712676]

(10). Li W; Wang F; Feng S; Wang J; Sun Z; Li B; Li Y; Yang J; Elzatahry AA; Xia Y; Zhao D Sol-Gel Design Strategy for Ultradispersed TiO2 Nanoparticles on Graphene for High-Performance Lithium Ion Batteries. J. Am. Chem. Soc 2013, 135, 18300–18303. [PubMed: 24251981]

(11). Xiang Q; Yu J; Jaroniec M Synergetic Effect of MoS_2 and Graphene as Cocatalysts for Enhanced Photocatalytic H2 Production Activity of TiO2 Nanoparticles. J. Am. Chem. Soc 2012, 134, 6575–6578. [PubMed: 22458309]

(12). Shen J; Yan B; Shi M; Ma H; Li N; Ye M One Step Hydrothermal Synthesis of TiO_2-Reduced Graphene Oxide Sheets. J. Mater. Chem 2011, 21, 3415–3421.

(13). Geim AK Graphene Status and Prospects Science. Science 2009, 324, 1530–1534. [PubMed: 19541989]

(14). Li D; Kaner RB Graphene-Based Materials. Science 2008, 320, 1170–1171. [PubMed: 18511678]

(15). Mou Z; Wu Y; Sun J; Yang P; Du Y; Lu C TiO2 Nanoparticles-Functionalized N-Doped Graphene with Superior Interfacial Contact and Enhanced Charge Separation for Photocatalytic Hydrogen Generation. ACS Appl. Mater. Interfaces 2014, 6, 13798–13806. [PubMed: 25078680]

(16). Wang H; Dai H Strongly Coupled Inorganic-Nano-Carbon Hybrid Materials for Energy Storage. Chem. Soc. Rev 2013, 42, 3088–3113. [PubMed: 23361617]

(17). Liang Y; Li Y; Wang H; Dai H Strongly Coupled Inorganic/Nanocarbon Hybrid Materials for Advanced Electrocatalysis. J. Am. Chem. Soc 2013, 135, 2013–2036. [PubMed: 23339685]

(18). Cao X; Tian G; Chen Y; Zhou J; Zhou W; Tian C; Fu H Hierarchical Composites of TiO_2 Nanowire Arrays on Reduced Graphene Oxide Nanosheets with Enhanced Photocatalytic Hydrogen Evolution Performance. J. Mater. Chem. A 2014, 2, 4366–4374.

(19). Ng YH; Ikeda S; Matsumura M; Amal R A Perspective on Fabricating Carbon-Based Nanomaterials by Photocatalysis and Their Applications. Energy Environ. Sci 2012, 5, 9307–9318.

(20). Han X; Funk MR; Shen F; Chen Y-C; Li Y; Compbell CJ; Dai J; Yang X; Kim J-W; Liao Y; Connell JW; Barone V; Chen Z; Lin Y; Hu L Scalable Holey Graphene Synthesis and Dense Electrode Fabrication toward High-Performance Ultracapacitors. ACS Nano 2014, 8, 8255–8265. [PubMed: 25093751]

(21). Gómez-Navarro C; Weitz RT; Bittner AM; Scolari M; Mews A; Burghard M; Kern K Electronic Transport Properties of Individual Chemically Reduced Graphene Oxide Sheets. Nano Lett 2007, 7, 3499–3503. [PubMed: 17944526]

(22). Stankovich S; Dikin DA; Piner RD; Kohlhaas KA; Kleinhammes A; Jia Y; Wu Y; Nguyen ST; Ruoff RS Synthesis of Graphene-Based Nanosheets Via Chemical Reduction of Exfoliated Graphite Oxide. Carbon 2007, 45, 1558–1565.

(23). Zhang H; Lv X; Li Y; Wang Y; Li J P25-Graphene Composite as a High Performance Photocatalyst. ACS Nano 2010, 4, 380–386. [PubMed: 20041631]

(24). William G; Seger B; Kamat PV TiO2-Graphene Nanocomposites. UV-Assisted Photocatalytic Reduction of Graphene Oxide. ACS Nano 2008, 2, 1487–1491. [PubMed: 19206319]

(25). Akhavan O; Abudolahad M; Esfandiar A; Mohatashamifar M Photodegradation of Graphene Oxide Sheets by TiO_2 Nanoparticles after a Photocatalytic Reduction. J. Phys. Chem. C 2010, 114, 12955–12959.

(26). Radich JG; Krenselewski AL; Zhu J; Kamat PV Is Graphene a Stable Platform for Photocatalysis? Mineralization of Reduced Graphene Oxide with UV-Irradiated TiO2 Nanoparticles. Chem. Mater 2014, 26, 4662–4668.

(27). Qiu Y; Yan K; Yang S; Jin L; Deng H; Li W Synthesis of Size-Tunable Anatase TiO2 Nanospindles and Their Assembly into Anatase@Titanium Oxynitride/Titanium Nitride-Graphene Nanocomposites for Rechargable Lithium Ion Batteries with High Cycling Performance. ACS Nano 2010, 4, 6515–6526. [PubMed: 21038869]

(28). Wang X; Xiang Q; Liu B; Wang L; Luo T; Chen D; Shen G TiO2 Modified FeS Nanostructures with Enhanced Electrochemical Performance for Lithium-Ion Batteries. Sci. Rep 2013, 3, 2007. [PubMed: 23774372]

(29). Eda G; Mattevi C; Yamaguchi H; Kim H; Chhowalla M Insulator to Semimetal Transition in Graphene Oxide. J. Phys. Chem. C 2009, 113, 15768–15771.

(30). Larciprete R; Fabris S; Sun T; Lacovig P; Baraldi A; Lizzit S Dual Path Mechanism in the Thermal Reduction of Graphene Oxide. J. Am. Chem. Soc 2011, 133, 17315–17321. [PubMed: 21846143]

(31). Wang WF; He YL; Zhang MS; Yin Z; Chen Q Raman Scattering Study on Anatase TiO_2 Nanocrystals. J. Phys. D: Appl. Phys 2000, 33, 912–916.

(32). Xiang Q; Yu J; Jaroniec M Enhanced Photocatalytic H2-Production Activity of Graphene-Modified Titania Nanosheets. Nanoscale 2011, 3, 3670–3678. [PubMed: 21826308]

(33). Schniepp HC; Li J-L; McAllister MJ; Sai H; Herrera-Alonso M; Adamson DH; Prud'homme RK; Car R; Saville DA; Aksay IA, Functionalized Single Graphene Sheets Derived from Splitting Graphite Oxide. J. Phys. Chem. B 2006, 110, 8535–8539. [PubMed: 16640401]

(34). Radich JG; Kamat PV Making Graphene Holey. Gold-Nanoparticle-Mediated Hydroxyl Radical Attack on Reduced Graphene Oxide. ACS Nano 2013, 7, 5546–5557. [PubMed: 23641756]

(35). Zhao Y; Tang Y; Chen Y; Star A Corking Carbon Nanotube Cups with Gold Nanoparticles. ACS Nano 2012, 6, 6912–6921. [PubMed: 22797411]

(36). Tang Y; Burkert SC; Zhao Y; Saidi WA; Star A The Effect of Metal Catalyst on the Electrocatalytic Activity of Nitrogen-Doped Carbon Nanotubes. J. Phys. Chem. C 2013, 117, 25213–25221.

(37). Bai H; Jiang W; Kotchey GP; Saidi WA; Bythell BJ; Jarvis JM; Marshall AG; Robinson RA; Star A Insight into the Mechanism of Graphene Oxide Degradation Via the Photo-Fenton Reaction. J. Phys. Chem. C 2014, 118, 10519–10529.

(38). Zhao BX; Li XZ; Wang P 2,4-Dichlorophenol Degradation by an Integrated Process: Photoelectrocatalytic Oxidation and E-Fenton Oxidation. Photochem. Photobiol 2007, 83, 642–646. [PubMed: 17132072]

(39). Li W; Bai Y; Zhang Y; Sun M; Cheng R; Xu X; Chen Y; Mo Y Effect of Hydroxyl Radical on the Structure of Multi-Walled Carbon Nanotubes. Synthetic Met 2005, 155, 509–515.

(40). Gao W; Alemany LB; Ci L; Ajayan PM New Insights into the Structure and Reduction of Graphite Oxide. Nat. Chem 2009, 1, 403–408. [PubMed: 21378895]

(41). Zhou X; Zhang Y; Wang C; Xu X; Yang Y; Zheng B; Wu H; Guo S,; Zhang J. Photo-Fenton Reaction of Graphene Oxide a New Strategy to Prepare Graphene Quantum Dots for DNA Cleavage. ACS Nano 2012, 6, 6592–6599. [PubMed: 22813062]

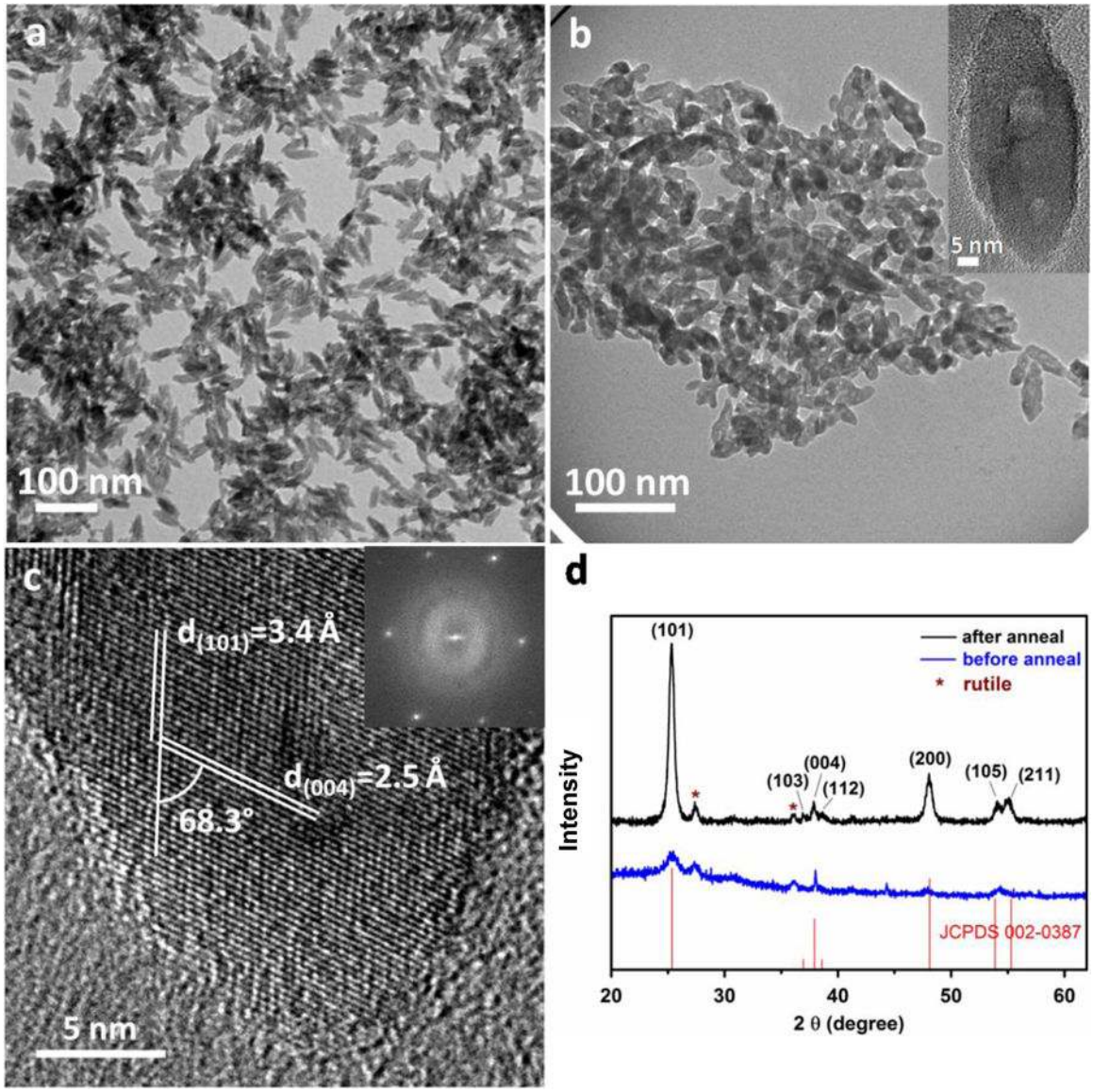

Figure 1.

Characterization of the TiO_2 nanospindles. (a, b) TEM image of TiO_2 nanospindles before (a) and after (b) annealing. Inset in panel b is TEM image of an individual TiO_2 nanospindle. (c) HRTEM image of an individual TiO_2 nanospindle. Inset is Fast Fourier Transform (FFT) of the HRTEM image. (d) The XRD patterns of the TiO_2 nanospindles before and after annealing in comparison to the standard anatase pattern (JCPDS 002–0387). * indicates rutile phase.

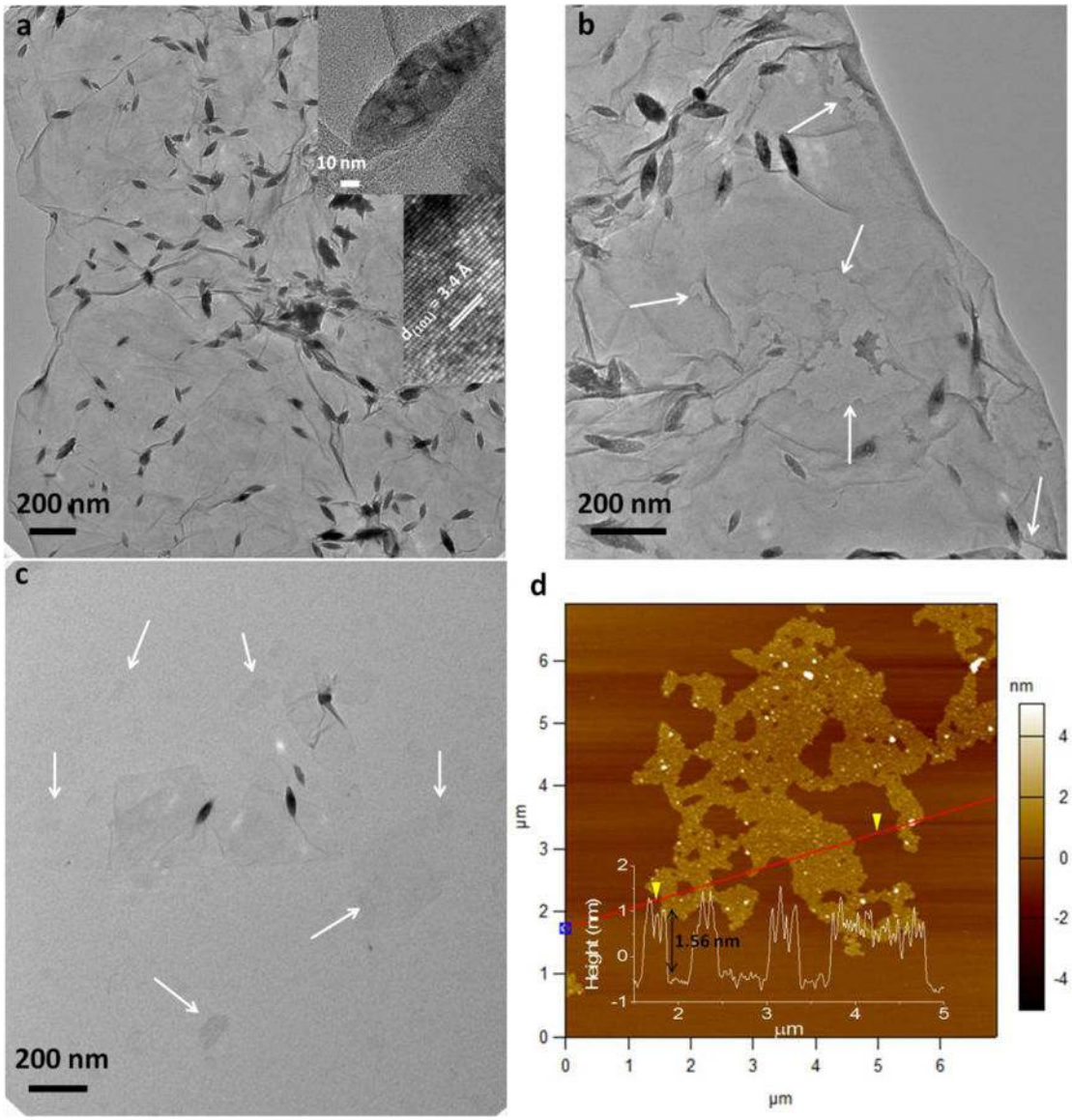

Figure 2.

Structural characterization of TiO_2 nanospindles/reduced graphene oxide. (a-c) TEM images of TiO_2/RGO at different photodegradation stages. (a) 0 h, (b) 8 h, (c) 18 h. (d) AFM image of TiO_2/RGO after 8 h photodegradation. Inset in (d) is the height profile between the two yellow triangles along the red line.

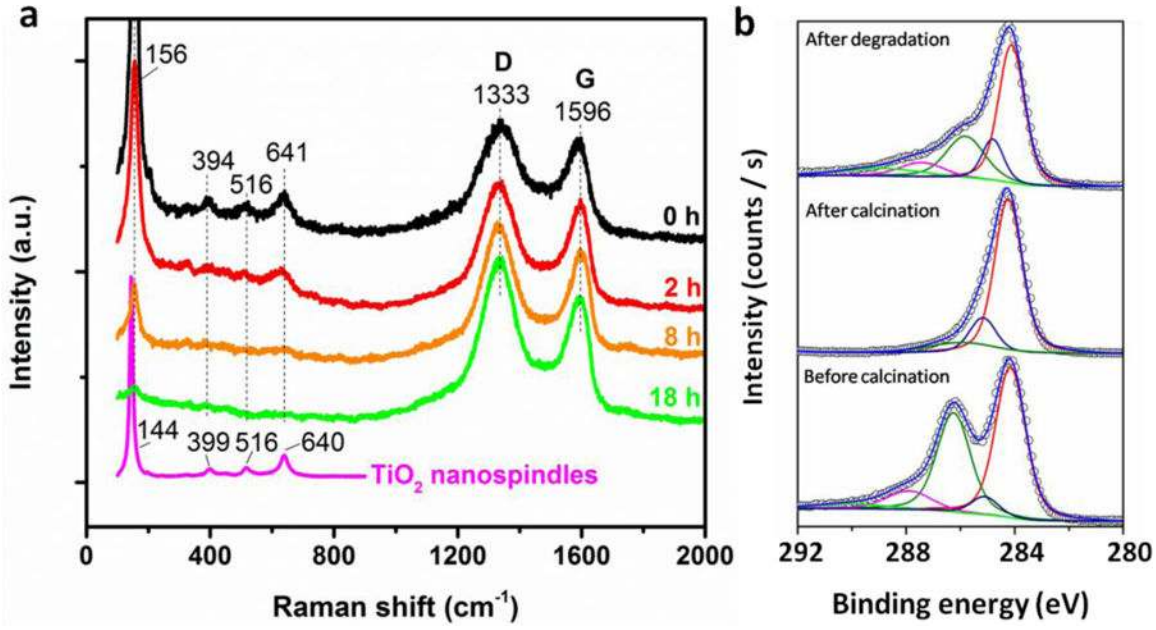

Figure 3.

Spectroscopic characterization of nanostructures. (a) Raman spectra of TiO_2 nanospindles and TiO_2/RGO at different photodegradation stages. (b) C1s XPS spectra of TiO_2/GO, TiO_2/RGO, and TiO_2/hRGO before calcination (TiO_2/GO), after calcinations (TiO_2/RGO) and after 18 h photodegradation.

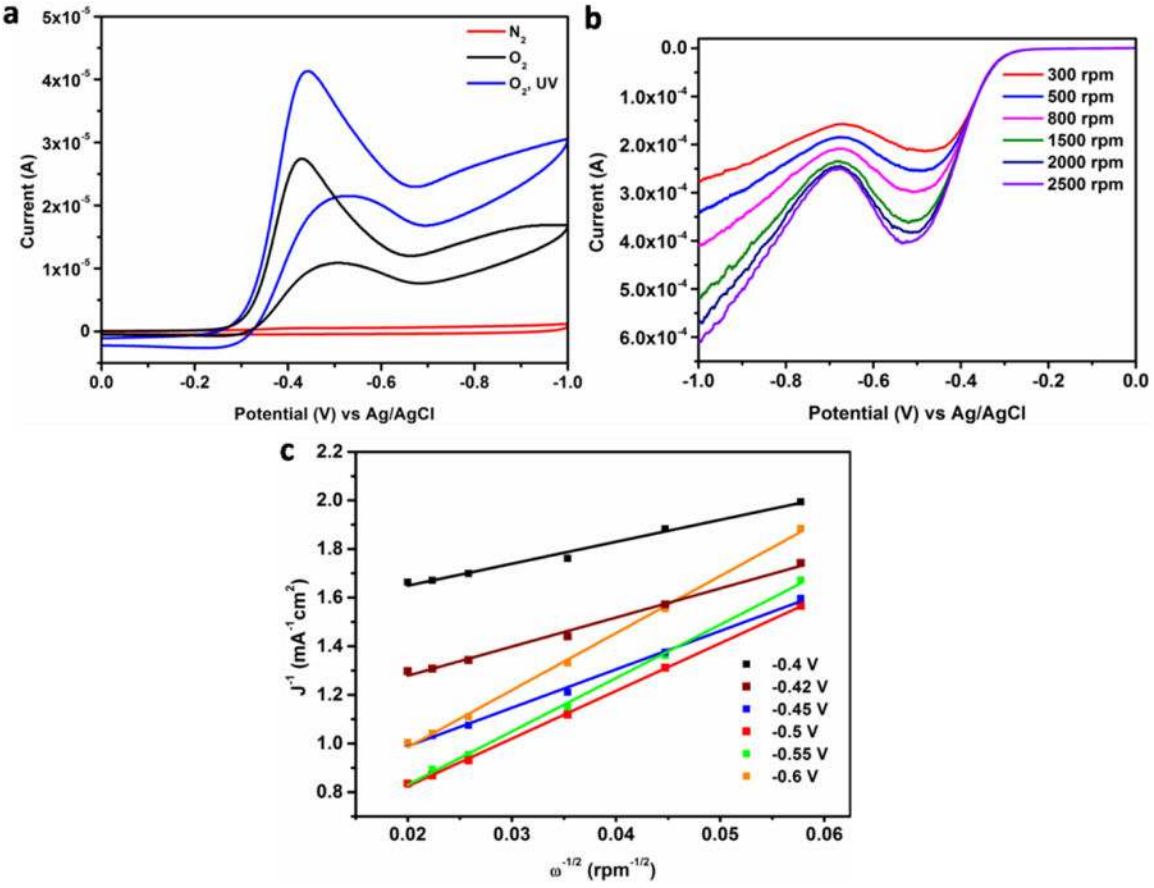

Figure 4.

(a) Cyclic voltammograms (CV) of TiO_2 nanospindles with (blue curve) and without (black curve) UV light irradiation in 0.1 M KOH aqueous solution. The red curve is obtained in N_2 saturated 0.1 M KOH without UV light. (b) Linear sweep voltammograms (LSV) for TiO_2 nanospindles on rotating ring disk electrode at various rotating rates in O_2 saturated 0.1 M KOH. (c) Koutecky-Levich plots for TiO_2 nanospindles obtained from the LSV curves in (b) at different potentials.

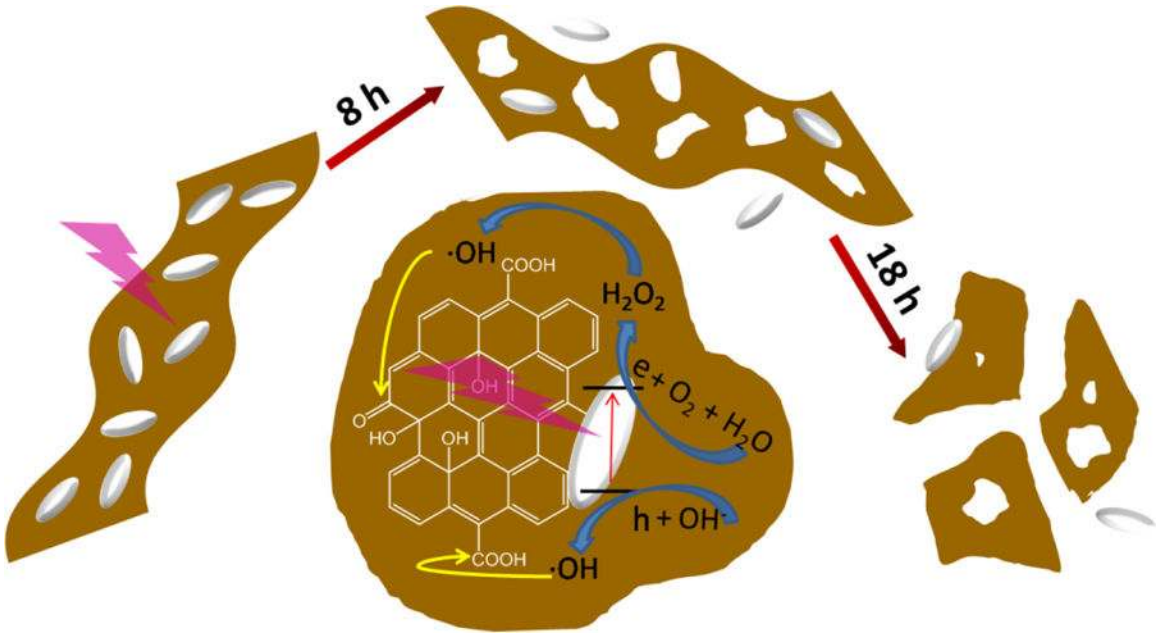

Figure 5.
Schematic illustration of TiO_2/holey graphene oxide evolution process.